Kepler Instrument Performance: an In-flight Update

Douglas A. Caldwell*[a] Jeffrey E. Van Cleve[a] Jon M. Jenkins[a] Vic S. Argabright[b] Jeffery J. Kolodziejczak[c] Edward W. Dunham[d] John C. Geary[e] Peter Tenenbaum[a] Hema Chandrasekaran[a,f] Jie Li[a] Hayley Wu[a] Jason Von Wilpert[g]

[a]SETI Institute/NASA Ames Research Center, MS 244-30, Moffett Field, CA 94035;
[b]Ball Aerospace & Technologies Corp.,1600 Commerce Street, Boulder, CO 80301;
[c]NASA Marshall Space Flight Center, VP60, Huntsville, AL 35812;
[d]Lowell Observatory, 1400 West Mars Hill Road, Flagstaff, AZ 86001;
[e]Smithsonian Astrophysical Observatory, 60 Garden St., Cambridge, MA 02138;
[f] Lawrence Livermore National Laboratory, 7000 East Avenue Livermore, CA 94550-9698;
[g] Affiliation2, Address, City, Country;

ABSTRACT

The Kepler Mission is designed to detect the 80 parts per million (ppm) signal from an Earth-Sun equivalent transit. Such precision requires superb instrument stability on time scales up to 2 days and systematic error removal to better than 20 ppm. The sole scientific instrument is the Photometer, a 0.95 m aperture Schmidt telescope that feeds the 94.6 million pixel CCD detector array, which contains both Science and Fine Guidance Sensor (FGS) CCDs. Since Kepler's launch in March 2009, we have been using the commissioning and science operations data to characterize the instrument and monitor its performance. We find that the in-flight detector properties of the focal plane, including bias levels, read noise, gain, linearity, saturation, FGS to Science crosstalk, and video crosstalk between Science CCDs, are essentially unchanged from their pre-launch values. Kepler's unprecedented sensitivity and stability in space have allowed us to measure both short- and long-term effects from cosmic rays, see interactions of previously known image artifacts with starlight, and uncover several unexpected systematics that affect photometric precision, including unexplained diffuse illumination events that occur at significant levels 10 times per month. Based on these results, we expect to attain Kepler's planned photometric precision over 90% of the field of view.

Keywords: *Kepler Mission*, exoplanets, photometry, space telescopes

1. INTRODUCTION

The Kepler Mission has been observing a 115 square degree field of view (FOV) in Cygnus centered at RA = 19h 22m 40s, Dec = 45d 30' since May 2009 in search of transiting extrasolar planets.[1] The primary goal of the Kepler mission is to measure the frequency of Earth-size planets orbiting in the habitable zones of Sun-like stars.[2] In order to meet this goal, the mission uses a wide-field photometer designed to give 20 part per million (ppm) photometric precision on 12th magnitude stars in 6.5 hours over timescales of order 2 days. The instrument also needs to have a very high duty cycle to allow for nearly continuous viewing and to be sufficiently stable over timescales of years so that the precision over 2 day timescales does not degrade significantly. The photometer uses a 0.95 m aperture Schmidt telescope and a focal plane with 42 CCD detectors totaling 96 million pixels on the sky. Details of the instrument design, construction and testing are given elsewhere.[1,3,4] Early results from Kepler indicate that the instrument is performing as designed[5] and that we are getting both the photometric precision and the instrument stability necessary to meet Kepler's goals.[6,7] However, the presence of several image artifacts put some parts of the focal plane at risk to achieving the precision needed to find Earth-size transits.[5]

In this paper we give an updated report on the in-flight detector properties after nearly a year of operations for comparison with those found in the *Kepler* Instrument Handbook.[4] Sec Y contains a detailed description

*douglas.caldwell@nasa.gov

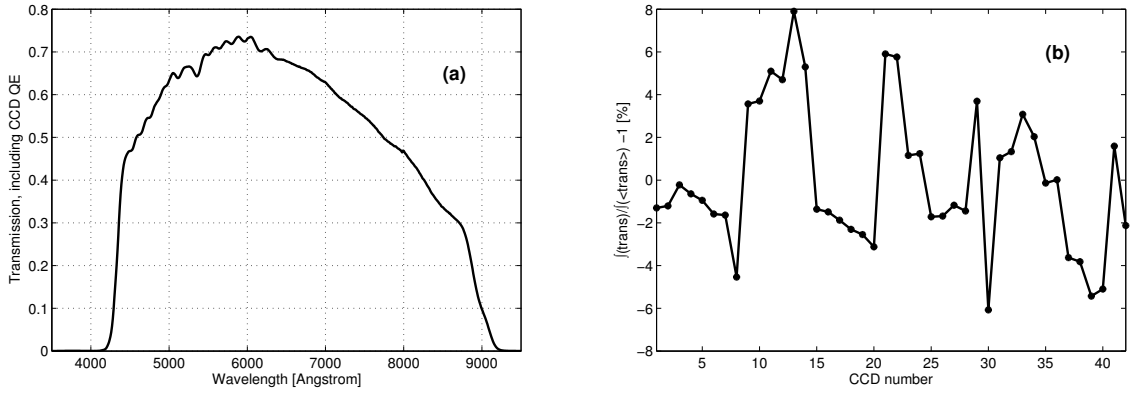

Figure 1: *Kepler* total relative transmission including CCD QE. Panel (a), mean transmission over all channels on the focal plane. Panel (b), relative integrated transmission difference from mean transmission for each of the 42 CCDs. The maximum integrated transmission difference is 8%, not including vignetting, which is up to 11% at the edge of the field of view.

of the image artifacts and other quirks of the instrument that are revealed by observing with such precision. Sec Z describes the artifact mitigation steps that have been developed and are being deployed to the Science Operations Center (SOC) data processing pipeline.[8]

2. TELESCOPE AND OPTICS PERFORMANCE

The *Kepler* spacecraft consists of a Schmidt telescope mounted on the spacecraft bus. The Schmidt telescope consists of a 1.4 m primary mirror, a 0.95 m fused-quartz corrector plate, and 25 sapphire field-flattener lenses (FFL) at the focal plane. The focal length of 1.4 m results in science field-of-view (FOV) of over 115 square degrees and a plate scale of 3.98 arcseconds/pixel. Because of the large FOV, the optical point-spread-function (PSF) varies significantly over the focal plane, even at "best focus." The focus set point was chosen to attempt to minimize the diameter containing 95% of the PSF's encircled energy across the focal plane. However, the *Kepler* project was conservative in operating the focus mechanisms –one of the few moving parts in the spacecraft– and thus also wanted to minimize the number of focus adjustments. The spacecraft was launched with the mirror at the predicted in-flight best focus position, but once the photometer thermalized in-flight it was determined that the achieved point-spread function would result in being able to monitor only $\sim 130,000$ of the 170,000 stars for which the mission was designed. The final focus state was arrived at by two moves: a piston of 40 μm and a tip-tilt. The resulting 95% encircled energy diameters range from 3.2 to 7.5 pixels. Seasonal temperature variations of the photometer result in changes of up to $\pm 10\%$.[9]

2.1 Transmission and Quantum Efficiency

In order to meet its precision requirement of 20 ppm, the *Kepler* photometer needs to collect 4.6×10^9 electrons in 6.5 hours from a 12^{th} magnitude star. This precision requirement set the aperture size, transmission and quantum efficiency (QE) requirements for the photometer. Based on measurements of the Sun, a noise level of 10 ppm relative to a 12^{th} magnitude star has been allocated to stellar variability.

The *Kepler* focal plane consists of 21 modules, each with one field-flattener lens, which serves as the bandpass filter, and two CCDs. *Kepler's* focal plane average transmission curve is shown in Figure 1, along with the relative variation in integrated transmission for each of the 42 CCDs. The in-flight mean flux for 12^{th} stars is 4.59×10^9 electrons in 6.5 hours,[7] within 1% of the pre-launch prediction. The transmission curves in Figure 1 do not include geometric vignetting, which is less than 1% within 4.6 degrees of the center and increases to 11% at the edge of the FOV at 6.94 degrees off-axis. While the vignetting is independent of wavelength, there is color dependent variation over the focal plane caused by differences among the bandpass filters on the FFLs and by

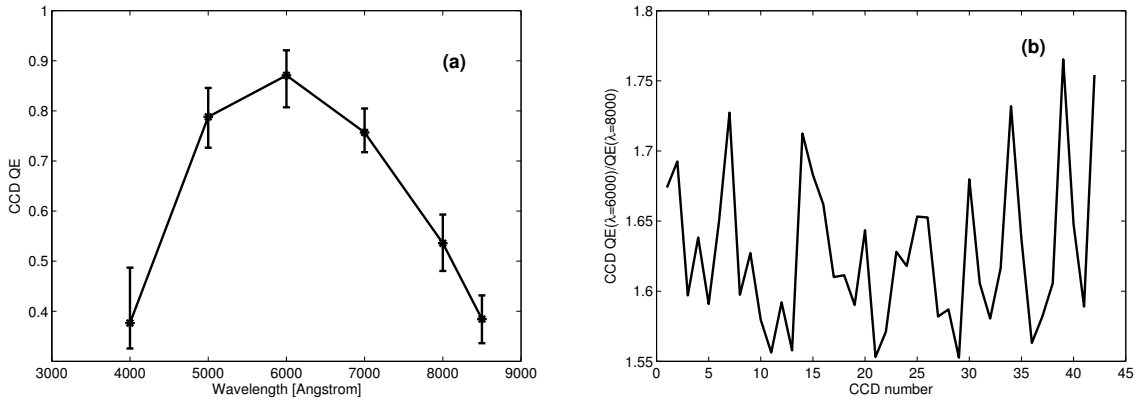

Figure 2: *Kepler* CCD QE over all CCDs on the focal plane. Panel (a) – mean QE over all CCDs. The error bars give the full range (max-min) of QE at each measured wavelength. Panel (b)– ratio of QE(6000Å)/QE(8000Å). The ratio varies from the mean ratio of 1.63 by −5% to +8% with an rms scatter of 3%.

differing CCD QE. The mean CCD QE is shown in Figure 2a. A measure of the color-dependent variation in QE is given in Figure 2b, which gives the ratio of QE at 6000 Å to the QE at 8000 Å. These wavelengths correspond roughly to the emission peak wavelength of a G5 star (T = 4800 K), and an M0 star (T = 3600 K); therefore, variations in the QE ratio of order 5% give an indication of the variations in relative response between G and M stars over the focal plane.

2.2 Scattered Light and Ghosting

Scattered light and ghosting generate optical crosstalk between stars on the focal plane and serve as a noise source in *Kepler* data. The levels of several scattered light and ghosting signals were modeled and measured prior to launch and were expected to be low enough to meet *Kepler's* precision requirements over 99% of the field of view. The most significant scattering and ghosting signals are given in Table 1, along with the log of the ratio of the scattered light/ghost signal to the source. Multiple the values by 2.5 to convert to astronomical magnitudes.

Table 1: Major scattered light and ghosting sources and relative signal levels.

Scattering/Ghost Source	**$\log_{10}$ of relative signal**
light scattered from the telescope structure (from objects in the FOV, or from objects outside the FOV –primarily Jupiter and the Earth)	-6 *predicted*
light scattered from the gaps between modules on the focal plane	-8.9
light scattered from the gaps between the CCDs on a module	-5.4, *predicted*
light scattered from the surface of the aluminum mask over the first 20 rows of each CCD	-4.3
specular scattering from the edge of the CCD	-4.5
specular scattering from the edge of the aluminum mask	-3.8
FFL surface ghosts	
Schmidt corrector ghost	-3.9

Objects outside the FOV scatter light diffusely over the entire focal plane. The combined signal from Earth

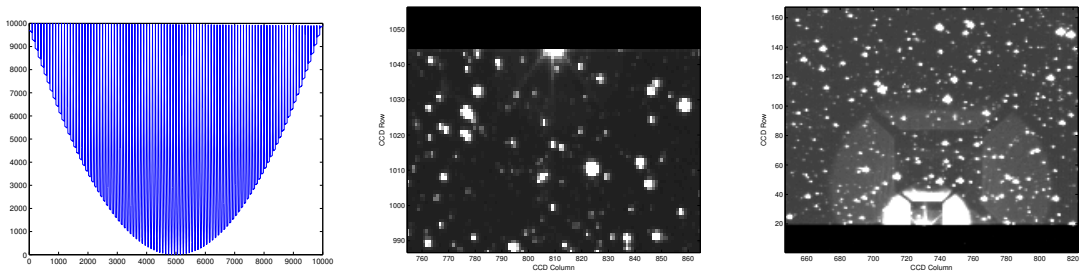

Figure 3: Scattered light from features on the focal plane: (a) module gaps (b) CCD edge (c) CCD mask

and Jupiter was expected to be lower than 23.3 e^- $pixel^{-1}$ sec^{-1}, or less than 1 ppm for a magnitude 12 target star. The scattered light from sources outside of the FOV has not yet been measured in flight, but with more than a year of data now available, we should be able to separate the scattered light signal from zodiacal light and other diffuse background sources.

Three of the focal plane scattering types are observed in flight as shown in Figure 3. The largest observed signals are $\sim zzz$ e^- sec^{-1}, or $\sim 0.0w\times$ the source signal. Because the scattering is off of an edge for these sources, the levels depend sensitively on the precise location of the scattering source. In addition to being modulated by pointing changes, these scattering signals will be modulated by the variability of the source stars. While this effect has not been measured for any *Kepler* targets, it is expected to be a source of noise for approximately qq% of the FOV, based on the extent of the scattered light signal around the edge of the CCDs.

There are three optical ghosts that produce a significant signal on the *Kepler* focal plane (see Figure 4): (1) a reflection off of the CCD surface, off the back (nearest the CCD) surface of the FFL and back to the CCD, (2) off the CCD surface, off the FFL front surface and back to the CCD, and (3) reflection off of the CCD, off of the Schmidt corrector and back to a CCD across the focal plane.

In Quarter-1, the star shown in Figure 4 (Kepler 9528112) had a measured flux of 6.2×10^7 e^- sec^{-1}, corresponding to a measured Kepler magnitude of 5.8 (the star has a Kepler Input Catalog Kepler magnitude Kp=6.8). The total flux in the FFL ghost is $\sim 2\%$ of the source flux, but it is spread over approximately 2000 pixels, so the ghost flux per pixel is $\sim 1 \times 10^{-5}$ times the source flux. The ghost off of the front surface of the FFL is spread over nearly twice the area of the back surface ghost and is thus considerably fainter and only detectable for the few brightest stars on the focal plane. The ratio of the flux in the Schmidt corrector ghost to the source flux in this image is $\sim 4 \times 10^{-4}$, or a log ratio of -3.4, compared with the pre-launch measure of -3.9.

2.3 Background Flux

The background flux seen by *Kepler* comes primarily from two sources: zodiacal light from the solar system and diffuse starlight from faint background stars. The pre-launch predictions of the background level used a value of 334 e^- sec^{-1}, based on an assumption that the zodiacal light plus diffuse star background light is equivalent to one 22^{nd} magnitude star per square arcsecond.

In order to measure the background level, the *Kepler* project places $\sim$ 4400 pixels in 2×2 apertures in an approximate grid on each of the 84 detector channels. The background observations are taken at the long cadence rate.The background level for a given star is determined from a 2D polynomial fit to the measured background pixel values. Observations since *Kepler's* launch show that there are comparable background contributions from the zodiacal and Galactic sources. For a given instant in time, the measured background flux varies smoothly as a function of Galactic latitude (see Figure 5). In Quarter-3 (*Kepler's* Fall roll orientation), the background values range from 140e^- sec^{-1} to 250 e^- sec^{-1}, or $\sim$ 7 to 14 DN/read. While in Quarter-4 the background ranges from 190 to 330 e^- sec^{-1}, or $\sim$ 10 to 18 DN/read. The time variation of the background level for one sky location is dominated by the changing zodiacal light as *Kepler* orbits the sun. The time varying signal near the center of the FOV varies from 156 to 250 e^- sec^{-1}, as seen in Figure 6. The variation of $\sim$ 50 e^- sec^{-1} seen

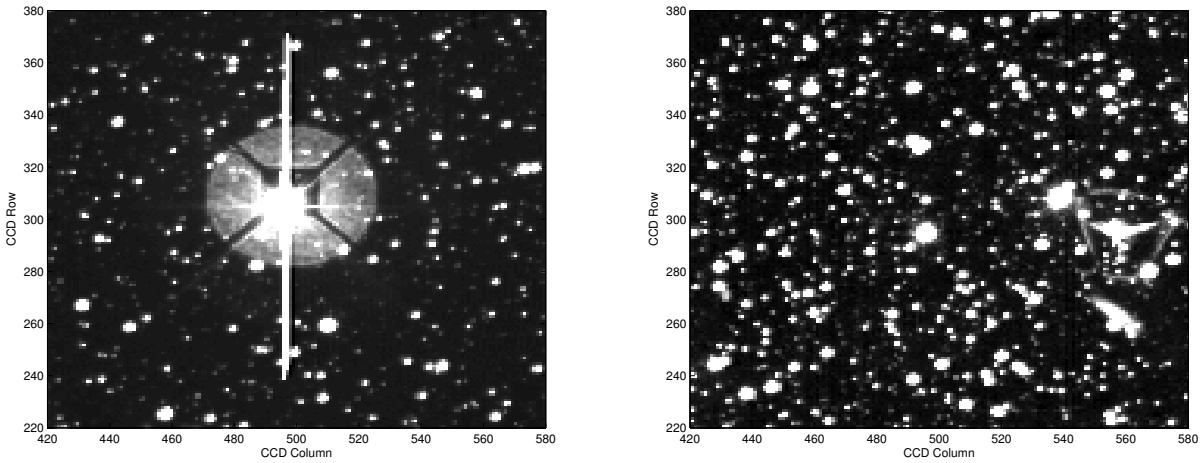

Figure 4: Sample optical ghost images: (a) FFL ghost seen around a bright star (Kepler 9528112, V* AF Cyg), left panel, and (b) Schmidt corrector ghost across the focal plane caused by this same star (centered around row, column = (300,560), right panel. The visible FFL ghost is off of the back surface of the lens. It is spread over $\sim$ 2000 pixels and clearly shows an image of the central obscuration and support spider. The ghost off of the front surface of the FFL is not visible for this source. The Schmidt corrector ghost has a trefoil shape, indicating that the corrector plate is likely under some stress. This ghost is not exactly symmetrically across the focal plane, rather is has a 60 pixel, or 4 arcmin, offset for this pair of channels due to slight variations in locations and orientations of the individual focal plane modules.

in Figure 5 for this location (the corner of the center module nearest the Galactic plane) between Quarter-3 and Quarter-4 can be accounted for by the difference in the time varying zodiacal signal, which has a peak-to-peak variation of ~ 90 e$^-$ sec^{-1} on a mean signal of 180 e$^-$ sec^{-1}.

3. FOCAL PLANE ARRAY PERFORMANCE

3.1 Noise

3.2 Gain and Linearity

3.3 Crosstalk

3.3.1 Video to Video Crosstalk

3.3.2 Clock to Video Crosstalk

3.4 Image Artifacts

3.4.1 LDE Undershoot

3.4.2 2D Black Artifacts

3.4.3 Pixel Defects

3.5 Thermal Stability

3.6 Timing Accuracy & Stability

ACKNOWLEDGMENTS

We gratefully acknowledge the years of work by the many hundred members of the Kepler Team who con- ceived, designed, built, and now operate this wonderful mission. Funding for the *Kepler Mission* is provided by NASA's Science Mission Directorate.

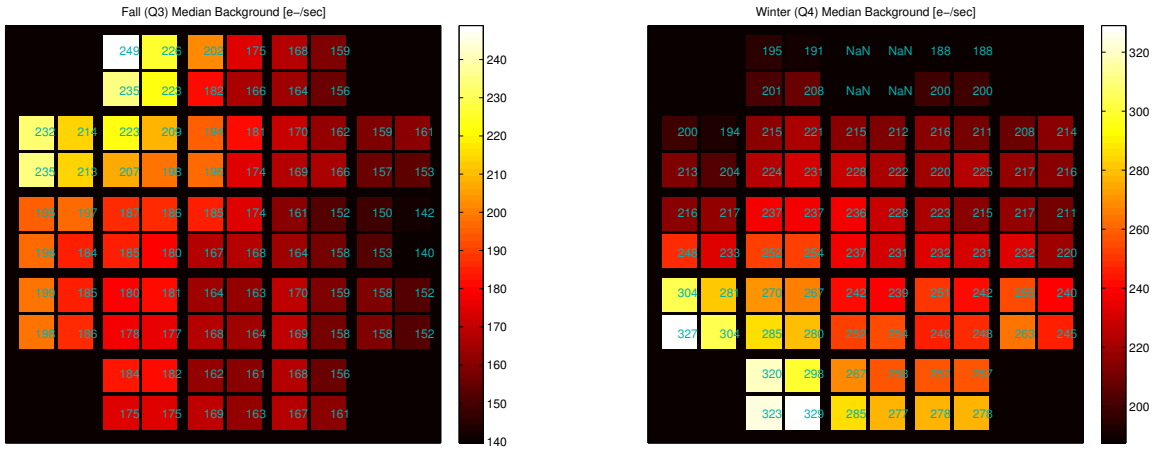

Figure 5: Median Background level measured over the focal plane for two different orientations of the photometer (a) Fall 2009 (Quarter-3), left panel and (b) Winter 2009/2010 (Quarter-4), right panel. The median over time of the background flux value for each output channel is shown in units of electrons/sec. In Quarter-3, the Galactic plane is oriented near the upper left of the focal plane. In Quarter-4 the Galactic plane is oriented near the lower left of the focal plane. Note that Module-3 (top row center) failed during Quarter-4, so there are no valid background measurements for this module.

REFERENCES

1. Koch, D. G. *et al.*, "*Kepler* mission design, realized photometric performance, and early science," ApJ Lett. 713(2), L79-L86 (2010).
2. Borucki, W. J. *et al.*, "*Kepler* planet-detection mission: introduction and first results," Science 327, 977-980 (2010).
3. Argabright, V. S. *et al.*, "The *Kepler* photometer focal plane array," Proc. SPIE 7010 (2008).
4. Van Cleve, J., & Caldwell, D. A. 2009, Kepler Instrument Handbook, KSCI 19033-001 (Moffett Field, CA: NASA Ames Research Center), `http://archive.stsci.edu/kepler/`
5. Caldwell, D. A. *et al.*, "Instrument performance in *Kepler's* first months," ApJ Lett. 713(2), L92-L96 (2010).
6. Borucki, W. J. *et al.*, "*Kepler's* optical phase curve of the exoplanet HAT-P7b," Science 325, 709 (2009).
7. Jenkins, J. M. *et al.*, "Initial characteristics of *Kepler* long cadence data for detecting transiting planets," ApJ Lett. 713(2), L120-L125 (2010).
8. Middour, C. *et al.*, "*Kepler* Science Operations Center architecture," Proc. SPIE 7740 in press (2010).
9. Bryson, S. T., *et al.* "The *Kepler* pixel response function," ApJ Lett. 713(2), L97-L102 (2010).

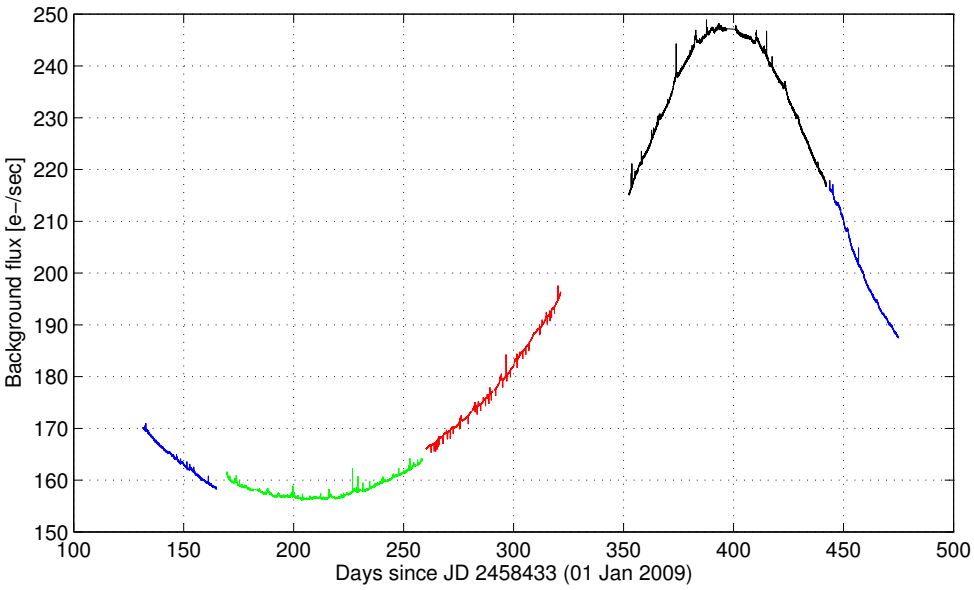

Figure 6: Time variation of Background level for a fixed sky location. The observations include approximately one year of background measurements from the central module in the focal plane, centered near ra, dec = ($19^{\rm h}27^{\rm m}$, $+44°30'$). The data from each roll orientation are indicated by color: Spring – blue, Summer – green, Fall – red, Winter – black. The seasonal variation is due to the changing zodiacal light signal as *Kepler* orbits the Sun and the angle between the Sun and the FOV changes. There are slight discontinuities at the seasonal rolls, because the data from the same portion of the sky are being collected on a different detector channel. Note that the background metric data are missing from the third month of the Fall orientation (near day 350). These data were successfully collected, but the background metrics were not calculated.